

# CHIRAL UNITARY APPROACH TO THE $N^*N^*\pi$ , $N^*N^*\eta$ COUPLINGS FOR THE $N^*(1535)$ RESONANCE

J.C. Nacher<sup>1,2</sup>, A. Parreño<sup>3</sup>, E. Oset<sup>1,2</sup>,  
A. Ramos<sup>4</sup>, A. Hosaka<sup>5</sup> and M. Oka<sup>6</sup>

<sup>1</sup> *Research Center for Nuclear Physics (RCNP), Osaka University, Ibaraki, Osaka 567-0047, Japan.*

<sup>2</sup> *Departamento de Física Teórica and IFIC, Centro Mixto Universidad de Valencia-CSIC 46100 Burjassot (Valencia), Spain.*

<sup>3</sup> *Institute for Nuclear Theory, University of Washington, Seattle, U.S.A.*

<sup>4</sup> *Departament d'Estructura i Constituents de la Matèria, Universitat de Barcelona, Diagonal 647, 08028 Barcelona, Spain.*

<sup>5</sup> *Numazu College of Technology, 3600 Numazu, 410-8501, Japan*

<sup>6</sup> *Department of Physics, Tokyo Institute of Technology, Meguro, Tokyo 152-8551, Japan*

## Abstract

Using a chiral unitary model in which the negative parity nucleon resonance  $N^* \equiv N^*(1535)$  is generated dynamically by means of the Bethe Salpeter equation with coupled meson baryon channels in the  $S = 0$  sector, we have obtained the  $\pi^0 N^* N^*$  and  $\eta N^* N^*$  couplings. The  $\pi^0 N^* N^*$  coupling has similar strength and the same sign as the  $\pi^0 N N$  coupling. This rules out the mirror assignment of chiral symmetry where the ground state nucleon  $N$  and the negative parity resonance  $N^*$  are envisaged as chiral partners in the baryon sector.

# 1 Introduction

Chiral symmetry has been playing a crucial role in understanding hadron physics. The current algebra and associated low energy theorems have been successfully applied to hadronic phenomena which in particular involve pions that appear as the Nambu-Goldstone bosons of spontaneous breakdown of chiral symmetry [1]. Recent developments of chiral perturbation methods for mesons and baryons are partly motivated by the hope in the theoretical side to describe hadrons without referring to particular models [2, 3, 4, 5, 6]. In Refs. [7, 8, 9], it was demonstrated that chiral perturbation theories, when unitarization in coupled channels is incorporated, can be applied up to resonance energy regions which are much beyond what the original chiral perturbation theories are supposed to be applied to. In Refs. [7, 8] this approach was referred to as the chiral unitary approach.

The advantage of the use of the chiral unitary approach is based on the implementation of exact unitarity together with a chiral expansion of  $\text{Re}(T^{-1})$  instead of the  $T$  matrix, in a way analogous to the effective range expansion in quantum mechanics. These manipulations allow one to extend the information contained in the chiral lagrangians with small number of derivatives to higher energies than expected.

In this way all meson resonances in meson meson scatterings up to 1.2 GeV were obtained [7,8]. Simultaneously an alternative but equivalent unitary approach was followed in [10] where the lowest order chiral Lagrangian was explicitly kept and the higher order one was generated from the exchange of genuine QCD resonances, following the idea of [11]. This allowed one to distinguish between genuine QCD resonances and other resonances which come as a consequence of the scattering of the mesons.

While a great success has been achieved in explaining hadron phenomena, several fundamental questions are not yet clearly answered. Here we would like to raise the following particular one concerning the formation of chiral multiplets: are there any particles which belong to the same chiral multiplets and so they will get degenerate when chiral symmetry is restored. In a linear sigma model, for instance, of  $SU(2) \times SU(2)$  chiral symmetry, a would-be chiral multiplet includes the  $\sigma$  and  $\pi$  mesons, which are the vector representations of the chiral group. In the spontaneously broken phase the pion becomes massless and the sigma meson remains massive, while in the symmetric phase they get degenerate and acquire an equal mass. Another candidate of a chiral multiplet is the pair of the vector ( $\rho$ ) and axial vector ( $a_1$ ) mesons. In both cases, the mass difference between particles in the same multiplet is considered to be generated by a finite scalar condensate associated with spontaneous break down of chiral symmetry.

For baryons, less attention has been paid in identifying them as members of chiral multiplets. For instance, one may ask what would be the chiral partner of the nucleon  $N(939)$ , and what

properties are dictated by the underlying chiral symmetry. In Refs. [12, 13], motivated by these questions, the chiral symmetry of the nucleon has been investigated, where two distinct chiral assignments for baryons were discussed. In one assignment, the positive and negative parity nucleons belong to different chiral multiplets, each of which is an independent representation of chiral symmetry. This case is referred to as the naive assignment. In the other case, positive and negative parity nucleons form a chiral multiplet, in which they transform to each other under chiral transformations. This case is referred to as the mirror assignment.

In both assignments, chiral symmetry puts unique constraints on properties of the positive and negative parity nucleons. In the naive assignment, a chiral symmetric lagrangian reduces to a sum of two lagrangians for positive and negative parity nucleons. Therefore, couplings between them disappear to leading order. In Ref. [13] this fact was considered to be the reason for the small coupling constant  $g_{\pi NN^*}$  for the decay of  $N^* = N^*(1535)$ . In contrast, in the mirror case, there are several interesting facts coming out. One of the non-trivial observations is that the positive and negative parity nucleons in the same chiral multiplet will get degenerate having a finite mass when chiral symmetry is restored. This and related properties lead to several interesting predictions on the behavior of the particle spectrum and interactions toward the restoration of chiral symmetry. For instance, the rate of meson production in nuclei depends crucially on the above chiral assignment [14].

One interesting signal which can be utilized to distinguish the two chiral assignments for the nucleon is the relative sign of the axial vector coupling constants. In the naive representation, their coupling constants take the same sign, while in the mirror representation they carry different signs. In reality, the physical nucleons can be combinations of the two representations, and therefore depending on the mixing rate their relative sign can be either positive or negative. If, however, the sign would be negative, the physical nucleons contain to a large extent the mirror component.

To our best knowledge up to date, the axial vector coupling constants of excited states have not been studied from the point of view of chiral symmetry. The main purpose of the present work is then to extract information theoretically on the sign of the axial vector coupling constant of the negative parity nucleon,  $N^*(1535)$ . We have chosen this state since it is the lowest negative parity state in nucleon excitations and would most likely be the chiral partner of the nucleon if any. Practically, it is convenient to compute the pion-baryon couplings, since they are related to the axial vector coupling constants through the Goldberger-Treiman relation. This is the main object in the present work. Since our interest is essentially related to chiral symmetry, it should be crucially important that the method adopted should respect chiral symmetry. In this respect, it is possible and looks appropriate to adopt a chiral unitary approach for the description of the negative parity nucleon  $N^*(1535)$ .

A chiral unitary approach to the meson baryon problem has been done in Ref. [15,16,17,18] using the Lippmann Schwinger [LS] equation and input from chiral Lagrangians. The  $\Lambda(1405)$  and  $N^*(1535)$  resonances are generated dynamically in those schemes in the  $S = -1$ ,  $S = 0$  channels, respectively. The connection between the inverse amplitude method and the Lippmann Schwinger equation (or better, the Bethe Salpeter equation) is done in [7], where a justification is found why in some channels, like in the case of  $\bar{K}N$  scattering in  $s$ -wave, the LS equation using the lowest order chiral Lagrangian and a suitable cut off in the loops can be a good approximation [18]. The procedure is not universal and in the case of the  $\pi N$  and coupled channel scatterings explicit use of the higher order Lagrangians is needed [17]. Alternatively one can use dispersion relations with different subtraction constants in each channel, which is the approach followed in [19] and the one which we will follow here. In both cases the  $N^*(1535)$  resonance is generated dynamically such that acceptable results for low energy cross sections for  $\pi N \rightarrow \eta N$  and related channels can be obtained.

This paper is organized as follows. In section 2, we briefly discuss the coupled channels chiral unitary approach for  $N^*(1535)$ . In section 3, we demonstrate how the strong couplings of the pion and eta to the resonance  $N^*(1535)$  are derived. There appear many diagrams which contribute to the relevant couplings. We investigate properties of all of these diagrams in detail. Numerical results are presented in section 4. We will find there that the  $\pi^0 N^* N^*$  coupling has similar strength and the same sign as the  $\pi^0 N N$  coupling. In section 5 we compare the present results with other model calculations. The final section is devoted to a summary and concluding remarks.

## 2 Chiral unitary approach to the $\pi N$ interaction and coupled channels

Let us consider the zero charge state with a meson and a baryon. The coupled channels in the  $S = 0$  sector are:  $\pi^- p$ ,  $\pi^0 n$ ,  $\eta n$ ,  $K^+ \Sigma^-$ ,  $K^0 \Sigma^0$ ,  $K^0 \Lambda$ . The lowest order chiral Lagrangian for the meson baryon interaction is given by [3,4,5]

$$\begin{aligned} L_1^{(B)} &= \langle \bar{B} i \gamma^\mu \nabla_\mu B \rangle - M_B \langle \bar{B} B \rangle \\ &+ \frac{1}{2} D \langle \bar{B} \gamma^\mu \gamma_5 \{u_\mu, B\} \rangle + \frac{1}{2} F \langle \bar{B} \gamma^\mu \gamma_5 [u_\mu, B] \rangle, \end{aligned} \quad (1)$$

where the symbol  $\langle \rangle$  denotes the trace of SU(3) matrices and

$$\begin{aligned} \nabla_\mu B &= \partial_\mu B + [\Gamma_\mu, B], \\ \Gamma_\mu &= \frac{1}{2} (u^+ \partial_\mu u + u \partial_\mu u^+), \\ U &= u^2 = \exp(i\sqrt{2}\Phi/f), \end{aligned} \quad (2)$$

$$u_\mu = iu^+\partial_\mu U u^+.$$

The SU(3) coupling constants which are determined by semileptonic decays of hyperons [20] are  $F \sim 0.46$ ,  $D \sim 0.79$  ( $F + D = g_A = 1.25$ ). The SU(3) matrices for the mesons and the baryons are the following

$$\Phi = \begin{pmatrix} \frac{1}{\sqrt{2}}\pi^0 + \frac{1}{\sqrt{6}}\eta & \pi^+ & K^+ \\ \pi^- & -\frac{1}{\sqrt{2}}\pi^0 + \frac{1}{\sqrt{6}}\eta & K^0 \\ K^- & \bar{K}^0 & -\frac{2}{\sqrt{6}}\eta \end{pmatrix}, \quad (3)$$

$$B = \begin{pmatrix} \frac{1}{\sqrt{2}}\Sigma^0 + \frac{1}{\sqrt{6}}\Lambda & \Sigma^+ & p \\ \Sigma^- & -\frac{1}{\sqrt{2}}\Sigma^0 + \frac{1}{\sqrt{6}}\Lambda & n \\ \Xi^- & \Xi^0 & -\frac{2}{\sqrt{6}}\Lambda \end{pmatrix}. \quad (4)$$

In order to describe  $N^*(1535)$  as a meson-baryon resonance state, we need interactions of the type  $MB \rightarrow MB$ . At lowest order in momentum, that we will keep in our study, the interaction Lagrangian comes from the  $\Gamma_\mu$  term in the covariant derivative and we find

$$L_{MB \rightarrow MB} = \langle \bar{B} i\gamma^\mu \frac{1}{4f^2} [(\Phi \partial_\mu \Phi - \partial_\mu \Phi \Phi) B - B (\Phi \partial_\mu \Phi - \partial_\mu \Phi \Phi)] \rangle. \quad (5)$$

This leads to a common structure of the type  $\bar{u} \gamma^\mu (k_\mu + k'_\mu) u$  for different meson-baryon channels, where  $u, \bar{u}$  are the Dirac spinors and  $k, k'$  the momenta of the incoming and outgoing mesons.

Simple algebraic manipulations of the amplitudes of eq. (5) allow us to write the lowest order amplitudes as

$$V_{ij} = -C_{ij} \frac{1}{4f^2} \bar{u}(p') \gamma^\mu u(p) (k_\mu + k'_\mu), \quad (6)$$

where  $p, p'(k, k')$  are the initial and final momenta of the baryons (mesons) and  $i, j$  indicate any of the channels mentioned above. Components of the symmetric matrix  $C_{ij}$  are given in Table 1. Since we are interested only in the  $s$ -wave part of the interaction, in which the  $N^*(1535)$  is generated, we can keep only the  $\gamma^0$  component of eq. (6) to a good approximation. This leads to a simple expression for the matrix elements

$$V_{ij} = -C_{ij} \frac{1}{4f^2} (k^0 + k'^0). \quad (7)$$

Following the steps of [18] we start from the Bethe Salpeter equation

$$t_{ij} = V_{ij} + V_{il} G_l t_{lj}, \quad (8)$$

where  $t_{ij}$  is the unitary transition matrix from channel  $j$  to channel  $i$  and  $G_l$  accounts for the intermediate meson and baryon propagators for the channel  $l$ . One of the interesting points proved in [18] is that the  $V$  and  $t$  matrices in that product appear with their on shell values,

Table 1:  $C_{ij}$  coefficients of eq. (6).  $C_{ji} = C_{ij}$ .

	$K^+\Sigma^-$	$K^0\Sigma^0$	$K^0\Lambda$	$\pi^-p$	$\pi^0n$	$\eta n$
$K^+\Sigma^-$	1	$-\sqrt{2}$	0	0	$-\frac{1}{\sqrt{2}}$	$-\sqrt{\frac{3}{2}}$
$K^0\Sigma^0$		0	0	$-\frac{1}{\sqrt{2}}$	$-\frac{1}{2}$	$\frac{\sqrt{3}}{2}$
$K^0\Lambda$			0	$-\sqrt{\frac{3}{2}}$	$\frac{\sqrt{3}}{2}$	$-\frac{3}{2}$
$\pi^-p$				1	$-\sqrt{2}$	0
$\pi^0n$					0	0
$\eta n$						0

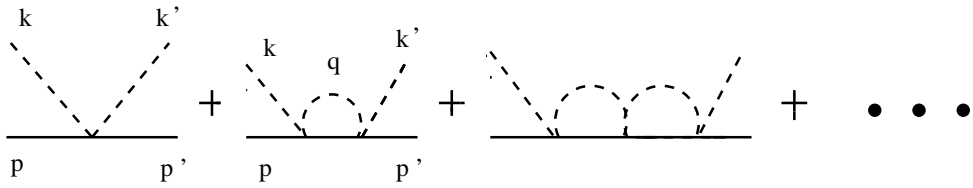


Figure 1: Diagrammatic representation of the Bethe Salpeter equation.

where the off shell part may be reabsorbed into renormalization of coupling constants of the lowest order Lagrangian. This feature was first found in [9] in the study of the scalar sector of the meson meson interaction. Hence, eq. (8) reduces to an algebraic equation where  $G$  is given by a diagonal matrix with matrix elements

$$G_l(s) = i \int \frac{d^4 q}{(2\pi)^4} \frac{M_l}{E_l(\vec{q})} \frac{1}{k^0 + p^0 - q^0 - E_l(\vec{q}) + i\epsilon} \frac{1}{q^2 - m_l^2 + i\epsilon}, \quad (9)$$

which depends on  $p^0 + k^0 = \sqrt{s}$  and  $q_{max}$ , the cut off which we choose for  $|\vec{q}|$  to regularize the loop integral of eq. (9).

The integral in eq. (9) without the cut off is logarithmically divergent. A subtraction of  $G_l(s')$  for a fixed value of  $s'$  makes it convergent but leads to an undetermined constant. The use of different subtraction constants in each of the channels is one way to account for SU(3) symmetry breaking, beyond the one provided by the unequal masses of the particles, and of effectively taking into account effects of higher order Lagrangians [10]. In this way we can then choose an alternative, and equivalent, way to account for this freedom by still evaluating  $G_l$  of eq. (9) with a cut off, equal for all channels and a subtraction constant. The cut off is taken larger than the on shell momenta of any particle in the intermediate states and in practice we take it  $q_{max} = 1$  GeV. Hence after performing analytically the  $q^0$  integration in eq. (9) we find

$$G_l = \int_{q_{max}=1 \text{ GeV}} \frac{d^3 q}{(2\pi)^3} \frac{1}{2\omega_l(q)} \frac{M_l}{E_l(\vec{q})} \frac{1}{p^0 + k^0 - \omega_l(\vec{q}) - E_l(\vec{q}) + i\epsilon} + a_l. \quad (10)$$

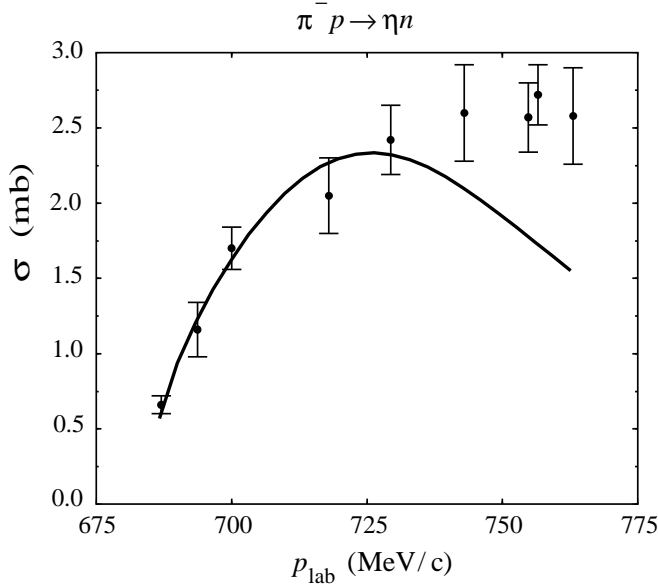


Figure 2: Cross section for  $\pi^- p \rightarrow \eta n$  reaction.

In order to keep isospin symmetry in the case that the masses of the particles in the same multiplet are equal, we choose  $a_l$  to be the same for states belonging to the same isospin multiplet. Hence we have four subtraction constants,  $a_{K\Sigma}$ ,  $a_{K\Lambda}$ ,  $a_{\pi N}$ ,  $a_{\eta N}$  which are considered free parameters and are fitted to the data. Simultaneously we take values of meson decay constants  $f$  different for  $\pi$  or  $K$ ,  $\eta$  couplings as is the case in  $\chi PT$  [2].

We find an acceptable solution to the low scattering data  $\pi^- p \rightarrow \eta n$ ,  $\pi^- p \rightarrow K^0 \Lambda$ ,  $\pi^- p \rightarrow K^0 \Sigma^0$  by means of the parameters:

$$f_\eta = f_K = 1.3 f_\pi, \quad f_\pi = 93 \text{ MeV (fixed)}, \quad (11)$$

$$q_{max} = 1 \text{ GeV (fixed)}, \quad (12)$$

$$a_{\pi N} = 98 \text{ MeV}, \quad a_{\eta N} = 18 \text{ MeV}, \quad a_{K\Lambda} = 34 \text{ MeV}, \quad a_{K\Sigma} = -30 \text{ MeV}. \quad (13)$$

As an example of the quality of the theoretical results, we show in Fig. 2 the cross section for  $\pi^- p \rightarrow \eta n$  reaction. Our method provides a fair reproduction of the low energy data, where the  $s$ -wave is dominant.

We find a pole for the  $N^*(1535)$  at  $1511 - i75$  MeV, which is compatible with a recent analysis of the data with a pole position at  $1510(\pm 10) - i85(\pm 15)$  MeV [21].

### 3 Scattering amplitude with $MB^*B^*$ Couplings

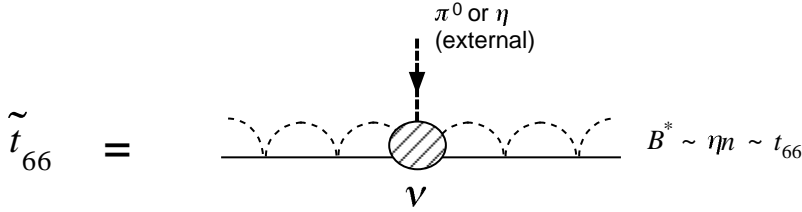


Figure 3: A diagram for the scattering amplitude of the meson( $M$ )-resonance( $B^*$ ) coupling  $\tilde{t}$ . For  $B^* \sim \eta n$ , the relevant matrix element is  $\tilde{t}_{66}$ .

### 3.1 General remarks

Meson-baryon resonance couplings are obtained by inserting an external meson line to the resonance state as shown in Fig. 3. The relevant scattering matrix is denoted as  $\tilde{t}_{ij}$ . We take external mesons as  $\pi^0$  and  $\eta$ . Furthermore, we specify the resonance state in the channel of  $\eta n$  which is purely isospin 1/2 and is largely dominated by the  $N^*(1535)$  pole. Therefore, following the ordering of the states in Table 1, the corresponding matrix elements are  $t_{66}$  and  $\tilde{t}_{66}$  for  $\eta n \rightarrow \eta n$  and  $\eta n \rightarrow \pi^0(\eta)\eta n$  respectively. There are several different ways for the meson insertion. Among them, we need to pick up those which have the resonance state both in the initial and final states. Therefore,  $\tilde{t}_{66}$  looks like

$$\tilde{t}_{66} \sim t_{66} \mathcal{V} t_{66}, \quad (14)$$

where  $\mathcal{V}$  represents the elementary vertex functions containing the external meson. There are three kinds of them as shown in Fig. 4:

**Fig. 4(a)** The point like three meson–baryon ( $BBMM$ ) vertex in which the external meson line is attached at the  $BBMM$  vertex of  $V_{ij}$ .

**Fig. 4(b)** The one connected through a meson-meson ( $M_1 M_2 \rightarrow M'_1 M'_2$ ) vertex.

**Fig. 4(c)** The one in which the external meson couples to the baryon in the meson-baryon propagator  $G_l$ . Although this diagram itself looks disconnected and irrelevant, after the inclusion of rescattering terms, it will become relevant for  $\tilde{t}_{66}$ .

Now by attaching  $t_{66}$  to the left and right of  $\mathcal{V}$ , we obtain  $\tilde{t}_{66}$ . First we consider the loop structure of  $\tilde{t}_{66}$ . The lowest order diagrams of them are shown in Figs. 5. There are new types of loop integrals. We can, however, simplify and relate them to that of the meson baryon propagator  $G_l$  of eq. (10) as follows:

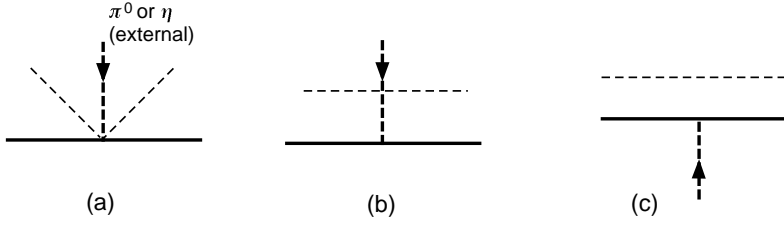


Figure 4: Diagrammatic representation for the vertex  $\mathcal{V}$  of Fig. 3. Although the diagram (c) is disconnected, after the inclusion of rescattering terms of  $t_{66}$ , it will become connected as shown in Fig. 5(c)

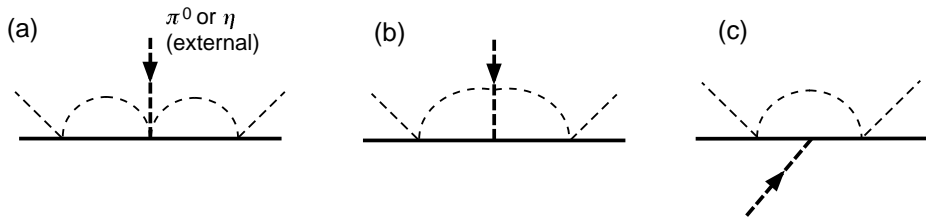


Figure 5: Vertex functions of  $\tilde{t}_{66}$  to lowest order in the rescattering. They are obtained by attaching  $t_{66}$  in the lowest order to the elementary diagrams given in Fig. 4.

Table 2: Diagonal coefficients  $x_{B'BM}$  and  $y_{B'BM}$  of eq. (16).

	$\Sigma^-$	$\Sigma^0$	$\Lambda$	$p$	$n$
$x_{BB\pi^0}$	-1	0	0	1	-1
$y_{BB\pi^0}$	1	0	0	0	0
$x_{BB\eta}$	$\frac{1}{\sqrt{3}}$	$\frac{1}{\sqrt{3}}$	$-\frac{1}{\sqrt{3}}$	$\frac{1}{\sqrt{3}}$	$\frac{1}{\sqrt{3}}$
$y_{BB\eta}$	$\frac{1}{\sqrt{3}}$	$\frac{1}{\sqrt{3}}$	$-\frac{1}{\sqrt{3}}$	$-\frac{2}{\sqrt{3}}$	$-\frac{2}{\sqrt{3}}$

**Fig. 5(a)** Given the structure of the three meson vertices which are factorized out from the integral, each loop integral of Fig. 5(a) reduces to that of the meson-baryon propagator  $G_l$ .

**Fig. 5(b)** The loop integrals here look new as they contain two meson propagators and one baryon propagator. However, the amplitudes of the diagrams (a) and (b) can combine in a way that one of the intermediate meson propagators of the diagram (b) cancels with part of the numerator coming from the  $MM \rightarrow MM$  amplitude yielding the same loop as  $G_l$ . This will be explained in Fig. 7.

**Fig. 5(c)** This diagram also looks new as it contains two baryon propagators and one meson propagator. Yet, we can show that in the case of static mesons which we will adopt here, this loop can be derived from  $G_l$  by differentiating with respect to a kinematical variable, similarly to what is done in quantum electrodynamics to derive the Ward identities.

### 3.2 $BBM$ vertex

In order to proceed, we investigate the structure of various vertices which appear in Figs. 4 and 5 in more detail. The simplest are the vertices of the Yukawa type ( $BB'M$ ) coupling. They are easily derived from the  $D$  and  $F$  terms of eq. (1) expanding  $U$  up to one meson field. We find in a non relativistic reduction of the  $\gamma^\mu\gamma^5$  matrix

$$-it_{B'BM} = A_{B'BM} \vec{\sigma} \cdot \vec{q}', \quad (15)$$

with

$$A_{B'BM} = \left\{ x_{B'BM} \frac{D+F}{2f} + y_{B'BM} \frac{D-F}{2f} \right\}, \quad (16)$$

where  $\vec{q}'$  refers to the momentum of the incoming meson  $M$ . The coefficients  $x_{B'BM}$  and  $y_{B'BM}$  are given in Table 2 for diagonal components. We need only diagonal matrix elements in the baryons, except for the possible case of  $\Sigma^0\Lambda\pi^0$  in which  $x_{\Sigma^0\Lambda\pi^0} = \frac{1}{\sqrt{3}}$  and  $y_{\Sigma^0\Lambda\pi^0} = \frac{1}{\sqrt{3}}$ .

Table 3:  $X_{lm}$  and  $Y_{lm}$  coefficients for the three meson vertex, eq. (19) for  $\pi^0$  coupling. They are diagonal as  $X_{lm} = X_{ml}$  and  $Y_{lm} = Y_{ml}$ .

	$X_{lm}$						$Y_{lm}$					
	$K^+\Sigma^-$	$K^0\Sigma^0$	$K^0\Lambda$	$\pi^-p$	$\pi^0n$	$\eta n$	$K^+\Sigma^-$	$K^0\Sigma^0$	$K^0\Lambda$	$\pi^-p$	$\pi^0n$	$\eta n$
$K^+\Sigma^-$	0	0	0	0	0	0	-2	0	0	0	$\frac{1}{\sqrt{2}}$	$\sqrt{\frac{3}{2}}$
$K^0\Sigma^0$		1	$-\frac{1}{\sqrt{3}}$	0	0	0		1	$-\frac{1}{\sqrt{3}}$	$-\frac{3}{\sqrt{2}}$	$-\frac{1}{2}$	$\frac{\sqrt{3}}{2}$
$K^0\Lambda$			-1	$\sqrt{6}$	$-\frac{1}{\sqrt{3}}$	1			-1	$-\sqrt{\frac{3}{2}}$	$\frac{1}{2\sqrt{3}}$	$-\frac{1}{2}$
$\pi^-p$				-4	$2\sqrt{2}$	0				0	0	0
$\pi^0n$					0	0					0	0
$\eta n$						0						0

### 3.3 $BBMM$ vertex

This vertex appears in the diagram Figs. 4(a) and 5(a). The Lagrangians for the three meson–baryon vertices are obtained expanding  $u_\mu$  in the  $F$ ,  $D$  terms of eq. (1) up to three meson fields. We obtain

$$u_\mu = \frac{\sqrt{2}}{12f^3} (\partial_\mu \Phi \Phi^2 - 2\Phi \partial_\mu \Phi \Phi + \Phi^2 \partial_\mu \Phi). \quad (17)$$

Expressions for the matrix elements of  $u_\mu$  involving only nucleons were obtained in [22]. Here we have to generalize it for the case of hyperons also. Once again, by taking the nonrelativistic approximation of the  $\gamma$  matrices,  $\gamma^\mu \gamma^5 \rightarrow \sigma^i$ , we obtain

$$-it_{\alpha'\alpha M} = C_{\alpha'\alpha M} \vec{\sigma} \cdot \vec{q}', \quad (18)$$

with

$$C_{\alpha'\alpha M} = \frac{1}{12f^2} (X_{\alpha'\alpha M} \frac{D+F}{2f} + Y_{\alpha'\alpha M} \frac{D-F}{2f}), \quad (19)$$

where the coefficients,  $X_{\alpha'\alpha M}$ ,  $Y_{\alpha'\alpha M}$ , with  $\alpha, \alpha'$  indicating a  $MB$  state, are given in Tables 3 and 4 for  $M \equiv \pi^0, \eta$  respectively.

In eqs. (18) and (19), we have kept only the terms which survive when  $t_{66}$  is attached to both sides of the three meson vertex, since the  $N^*$  state should be dynamically generated by the scattering of the meson. Note that the successive  $BBMM$ -vertices  $V_{ij}$ , where the incoming or outgoing meson is scattered, are  $s$ -wave couplings. Due to this  $s$ -wave nature, the terms in eq. (17) which involve the derivatives acting on the two internal mesons vanish in the loop integral and only the term which has the derivative in the external  $\pi^0$  or  $\eta$  field survives.

Table 4:  $X_{lm}$  and  $Y_{lm}$  coefficients for the three meson vertex, eq. (19) for  $\eta$  coupling. They are diagonal as  $X_{lm} = X_{ml}$  and  $Y_{lm} = Y_{ml}$ .

	$X_{lm}$						$Y_{lm}$					
	$K^+\Sigma^-$	$K^0\Sigma^0$	$K^0\Lambda$	$\pi^-p$	$\pi^0n$	$\eta n$	$K^+\Sigma^-$	$K^0\Sigma^0$	$K^0\Lambda$	$\pi^-p$	$\pi^0n$	$\eta n$
$K^+\Sigma^-$	0	$-\sqrt{3}$	-1	0	0	0	$-2\sqrt{3}$	$\sqrt{3}$	-1	0	$\sqrt{\frac{3}{2}}$	$\frac{3}{\sqrt{2}}$
$K^0\Sigma^0$		$-\sqrt{3}$	1	0	0	0		$-\sqrt{3}$	1	$\sqrt{\frac{3}{2}}$	$\frac{\sqrt{3}}{2}$	$-\frac{3}{2}$
$K^0\Lambda$			$\sqrt{3}$	$-\sqrt{2}$	1	$-\sqrt{3}$			$\sqrt{3}$	$\frac{1}{\sqrt{2}}$	$-\frac{1}{2}$	$\frac{\sqrt{3}}{2}$
$\pi^-p$				0	0	0				0	0	0
$\pi^0n$					0	0					0	0
$\eta n$						0						0

### 3.4 $MMMM$ vertex

Finally we consider the terms involving the meson meson interaction which appear in Figs. 4(b) and 5(b). The evaluation of the  $M_1 M_2 \rightarrow M'_1 M'_2$  vertices has been done in [9]. Here we need in addition the meson propagator and a  $B'BM$  vertex in order to evaluate the diagrams of Fig. 5(b) and its higher orders. Let us look in detail at these diagrams in some cases in order to see their general behavior.

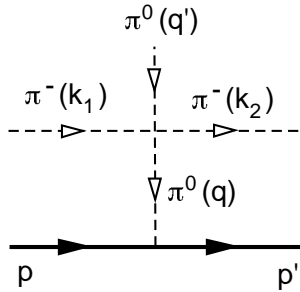


Figure 6: The case involving the  $\pi\pi \rightarrow \pi\pi$  vertex.

First let us take the case involving the  $\pi\pi \rightarrow \pi\pi$  vertex as shown in Fig. 6. The contribution of this diagram is:

$$-it = (-i) t_{\pi^-\pi^0 \rightarrow \pi^-\pi^0} \frac{i}{q^2 - m_\pi^2} \frac{D + F}{2f} \vec{\sigma} \cdot \vec{q}, \quad (20)$$

where

$$t_{\pi^-\pi^0 \rightarrow \pi^-\pi^0} = -\frac{1}{3f^2} [3(k_1 - k_2)^2 - \sum p_i^2 + m_\pi^2]. \quad (21)$$

We note that the  $\pi^-\pi^0 \rightarrow \pi^-\pi^0$  vertex function has an off shell behavior since it involves  $\sum p_i^2$  where  $p_i$  is the momentum of each of the pion lines. The first step is to recall that, following the steps of [9], the  $MM$  amplitude in the loops has to be taken with  $p_i^2 = m_i^2$ , since the terms

with  $p_i^2 - m_i^2$  will kill one of the off shell propagators and renormalize other diagrams already considered. This is illustrated in Fig. 7, where starting from diagram (a), the term  $k_1^2 - m_\pi^2$  would eliminate the internal meson propagator of momentum  $k_1$  and lead to diagram (b), which can be interpreted as a vertex correction of the three pion vertex, i.e., the diagram (a) of Fig. 4, as shown in the diagram Fig. 7(c). This can be reabsorbed into the physical coupling of the vertex of Fig. 4(a).

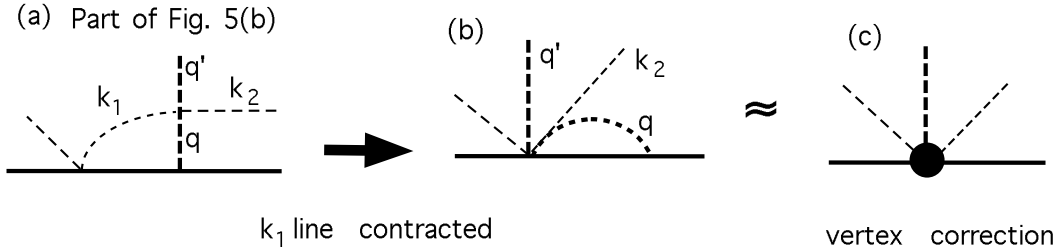


Figure 7: Diagram obtained from diagram Fig. 5(b) when the off shell part of the meson meson amplitude is considered.

Next we consider the first term of (21)

$$(k_1 - k_2)^2 = (q - q')^2. \quad (22)$$

In order to have the same kinematics of the  $N^*$  to the right and the left of the  $\pi^0 N^* N^*$  vertex we shall take  $q^\mu' \rightarrow 0$  (soft pion limit). We are concerned about the coefficient which will accompany  $\vec{\sigma} \cdot \vec{q}'$  for this vertex and this coefficient will be roughly independent of  $q'$  as is the case of the  $\pi NN$  vertex in the non relativistic limit that we take. Hence

$$(k_1 - k_2)^2 \simeq q^2 \quad (23)$$

in this limit. Keeping the other terms in eq. (22) would lead to  $q^2 + m_\pi^2$  since the linear term in  $q$  would vanish in the loops. The limit taken neglects  $m_\pi^2$  versus  $q^2$  which is certainly a fair approximation. Consistency with that approximation will require the neglect of the terms proportional to  $m_\pi^2$  when they appear and we shall do so in the evaluations here.

On the other hand the term  $\vec{\sigma} \cdot \vec{q}'$  in eq. (20) can be rewritten as:

$$\vec{\sigma} \cdot \vec{q}' = \vec{\sigma} \cdot (\vec{k}_1 + \vec{q}' - \vec{k}_2) \quad (24)$$

and the terms proportional to  $\vec{k}_1, \vec{k}_2$  will vanish in the loops. Hence we can write the contribution of the diagram of Fig. 6 in an effective way as:

$$-it = -\frac{1}{f^2} (q^2 - m_\pi^2) \frac{1}{q^2 - m_\pi^2} \frac{D + F}{2f} \vec{\sigma} \cdot \vec{q}' . \quad (25)$$

In this equation we see that the meson propagator cancels with the remnant of the  $\pi\pi \rightarrow \pi\pi$  vertex and we obtain a structure of the type of the three meson vertex of Fig. 5(a). Chiral symmetry brings always these two kind of diagrams together as is well known from early studies of  $\pi N \rightarrow \pi\pi N$  interaction [23] prior to the more systematic  $\chi PT$  approach to these amplitudes. The result obtained indicates that the contribution of these terms can be cast in the same way as in eq. (19).

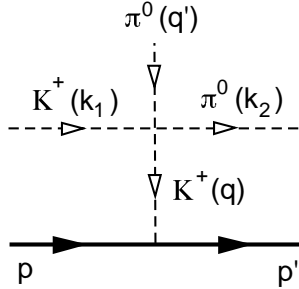


Figure 8: Feynman diagram for the  $K^+\pi^0 \rightarrow K^+\pi^0$  vertex.

Let us see another example shown in Fig. 8. In this case the  $K^+\pi^0 \rightarrow K^+\pi^0$  vertex, which we take from the  $K^+K^- \rightarrow \pi^0\pi^0$  amplitude of [9] via crossing, can be written after setting  $p_i^2 = m_i^2$  as:

$$-\frac{3}{4f^2}t = -\frac{3}{4f^2}(k_1 - q)^2 = -\frac{3}{4f^2}(k_2 - q')^2 \simeq -\frac{3}{4f^2}k_2^2, \quad (26)$$

and the on shell condition will render this as a term proportional to  $m_\pi^2$  which we will neglect. Note that in addition we would have one loop with two heavy meson propagators which would further reduce the strength of the diagram.

The argument above would lead to a term proportional to  $m_\eta^2$  if the  $\pi^0$  with momentum  $k_2$  is substituted by an  $\eta$ . This term would not be small in principle. However, the  $K^+$  attached to the baryon would involve the  $K^+\Sigma^- n$  vertex which goes like  $(F - D)$ , small compared to the  $F + D$  component. Furthermore it would involve two loops involving each two heavy mesons which would further reduce the contribution.

The arguments used above have been used in order to justify that terms of the type of Fig. 8 with a heavy meson exchange attached to the baryon line, with one loop to the right and another one to the left, should be small compared to those where just a pion is attached to the baryon line. We will just adopt this approximation and keep only the terms where a pion is exchanged there. Under these approximations the diagrams of the type of Figs. 6 and 8 can be cast in terms of an effective operator similar to eq. (19) as:

$$-it_{\alpha'\alpha M} = \tilde{C}_{\alpha'\alpha M} \vec{\sigma} \cdot \vec{q}', \quad (27)$$

Table 5:  $\tilde{X}_{lm}$  and  $\tilde{Y}_{lm}$  coefficients of eq. (28). They are diagonal as  $\tilde{X}_{lm} = \tilde{X}_{ml}$  and  $\tilde{Y}_{lm} = \tilde{Y}_{ml}$ .

	$X_{lm}$						$Y_{lm}$					
	$K^+\Sigma^-$	$K^0\Sigma^0$	$K^0\Lambda$	$\pi^-p$	$\pi^0n$	$\eta n$	$K^+\Sigma^-$	$K^0\Sigma^0$	$K^0\Lambda$	$\pi^-p$	$\pi^0n$	$\eta n$
$K^+\Sigma^-$	3	0	0	0	0	0	-3	0	0	0	0	0
$K^0\Sigma^0$		0	$-\sqrt{3}$	0	0	0		0	$-\sqrt{3}$	0	0	0
$K^0\Lambda$			0	0	0	0						
$\pi^-p$				-12	0	0				0	0	0
$\pi^0n$					0	0					0	0
$\eta n$						0						0

where

$$\tilde{C}_{\alpha'\alpha M} = \frac{1}{12f^2} \left( \tilde{X}_{\alpha'\alpha M} \frac{D+F}{2f} + \tilde{Y}_{\alpha'\alpha M} \frac{D-F}{2f} \right), \quad (28)$$

and the  $\tilde{X}$  and  $\tilde{Y}$  coefficients are given in Table 5 for an external  $\pi^0$  coupling. For the case of  $\eta$  external coupling and intermediate  $\pi$  attached for the baryon line, the  $MM \rightarrow MM$  vertices with three pions and one  $\eta$  are either zero or proportional to  $m_\pi^2$ , which we omit in our analysis. Surviving terms would involve loops with two kaons and  $\Sigma$  or  $\Lambda$  which should be suppressed. We will omit these terms and then within this approximation the  $\tilde{X}$ ,  $\tilde{Y}$  coefficients for the external  $\eta$  will be taken zero. In the case of the  $\eta$  the soft meson limit is also a drastic approximation. Altogether this means that for the  $\eta N^* N^*$  coupling we should admit larger uncertainties than for the  $\pi^0 N^* N^*$  coupling, where the approximations done are rather sensible.

In the end of this subsection, we note that in diagram (a), (b) of Fig. 5 we can sum the two contributions of the type of Fig. 4 (a), (b) in one block by means of

$$-t_{\alpha'\alpha'M} = D_{\alpha'\alpha M} \vec{\sigma} \cdot \vec{q}', \quad (29)$$

with

$$D_{\alpha'\alpha M} = \frac{1}{12f^2} \left[ (X_{\alpha'\alpha M} + \tilde{X}_{\alpha'\alpha M}) \frac{D+F}{2f} + (Y_{\alpha'\alpha M} + \tilde{Y}_{\alpha'\alpha M}) \frac{D-F}{2f} \right]. \quad (30)$$

## 4 Generation of the $\pi^0(\eta)N^*N^*$ vertex.

From the series of Fig. 3 we must pick up the terms which factorize the  $\eta n$  amplitude to the left and the right of the external  $\pi^0(\eta)$  vertex since this amplitude contains the  $N^*$  pole and hence the resulting amplitude can be compared to the conventional one which appears from the diagram of Fig. 9.

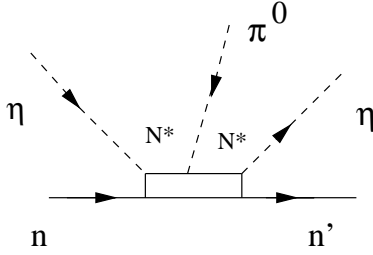


Figure 9: Diagrammatic representation of the  $\pi N^* N^*$  couplings with explicit  $N^*$  propagators.

Hence we shall start from  $\eta n$  in the series of Fig. 3 and finish up with  $\eta n$  for simplicity. The resulting amplitude will be compared to the one of Fig. 9 which is given by (the index 6 stands for the 6th channel of  $\eta n$  in Table 1)

$$-i\tilde{t}_{66}(\sqrt{s}) = (-ig) \frac{i}{\sqrt{s} - M^* + i\frac{\Gamma}{2}} C \vec{\sigma} \cdot \vec{q}' \frac{i}{\sqrt{s} - M^* + i\frac{\Gamma}{2}} (-ig), \quad (31)$$

where  $C \vec{\sigma} \cdot \vec{q}'$  is the  $N^* N^* \pi^0$  coupling, to be compared with  $-(D + F) \vec{\sigma} \cdot \vec{q}'/2f$  of  $\pi^0 nn$  in the case of nucleons. In eq. (31)  $g$  is the  $\eta n N^*$  coupling. On the other hand the  $\eta n \rightarrow \eta n$  amplitude proceeding through  $N^*$  excitation is depicted in Fig. 10 and given by

$$-it_{66}(\sqrt{s}) = (-ig) \frac{i}{\sqrt{s} - M^* + i\frac{\Gamma}{2}} (-ig). \quad (32)$$

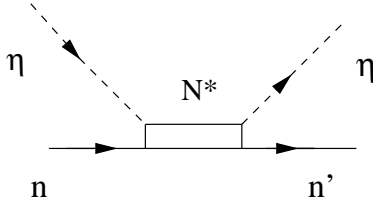


Figure 10: Diagrammatic representation of the  $\eta n \rightarrow \eta n$  process through explicit  $N^*$  excitation.

Our aim is to evaluate the coupling constant  $C$  in eq. (31). This will be accomplished by dividing by  $g^2$  and the square of the  $N^*$  propagator, information which will be obtained from eq. (32). We should note that the fact that the  $\eta N$  threshold (1486 MeV) is below the  $N^*$  mass (1511 MeV) makes the width  $\Gamma$  in eqs. (31, 32) strongly energy dependent, particularly close to the  $\eta N$  threshold. Hence  $t_{66}$  in eq. (32) differs from a Breit Wigner distribution close to the  $\eta N$  threshold but resembles it much better at energies above the  $N^*$  mass. This situation is shown in Figs. 11, where various scattering amplitudes are compared with the Breit-Wigner amplitudes. We can obtain  $g^2$  from eq. (32) by means of

$$g^2 = -\frac{\Gamma}{2} \text{Im} (t_{66}(M^*)), \quad (33)$$

where  $\Gamma$  is estimated by the relation

$$\text{Im} t_{66}(M^* + \frac{\Gamma}{2}) \simeq \text{Im} t_{66}(M^*)/2. \quad (34)$$

We find  $\Gamma = 140$  MeV,  $\text{Im } t_{66}(M^*) \simeq -0.1 \text{ MeV}^{-1}$  and hence  $g^2 \simeq 7$ . With this coupling we obtain a partial decay width of  $N^*$  into  $\eta n$  given by

$$\frac{\Gamma^{(\eta)}}{2} = \frac{g^2}{4\pi} \frac{M}{M^*} \bar{q} \quad (35)$$

with  $\bar{q}$  the  $\eta$  momentum in  $N^* \rightarrow \eta n$  and  $M$  the nucleon mass. For  $M^* = 1511$  MeV we obtain  $\Gamma^{(\eta)} = 90$  MeV and hence a branching ratio  $\Gamma^{(\eta)}/\Gamma_{tot} = 65\%$  a bit larger than the  $30 - 55\%$  quoted in the particle data table. However, a fine tuning of eq. (35) taking into account the mass distribution of the  $M^*$  reduces this  $N\eta$  partial decay width. Hence the coupling strength  $g^2 \sim 7$  we have obtained is sufficiently realistic for our purposes.

The amplitude  $\tilde{t}_{66}$  both for an external  $\pi^0$  and  $\eta^0$  behaves approximately as the square of a Breit Wigner distribution. Indeed, one should note that all the matrices  $t_{6l}$  contain the  $N^*$  pole. This can be seen from eq. (8) which reads in matrix form

$$t = [1 - VG]^{-1}V \quad (36)$$

and all matrix elements have a pole where  $\det[1 - VG] = 0$ , which occurs in the second Riemann sheet of the complex plane and corresponds to the  $N^*$  pole. Hence  $\tilde{t}_{66}$  should contain the  $N^*$  propagator squared as implied by eq. (31). However, we should also note that owing to the different backgrounds, the  $6 \times 6$  amplitudes which can be generated with the 6 states of Table 1 have slightly different shapes around the  $N^*$  energy and the peak of  $|\text{Im}(t)|$  fluctuates between 1510 MeV and 1520 MeV. As a consequence, the shapes of  $\tilde{t}_{66}$  for an external pion or eta are slightly different and also different from  $t_{66}^2$ , although all of them are qualitatively similar (see Figs. 11 (b), (c), (d) and (f)). For this reason, since close to the resonance pole the amplitudes change quickly, direct ratios of the  $\tilde{t}_{66}$  with  $t_{66}^2$  in order to obtain the constant  $C$  should not be done. Instead we find it proper to compare  $\text{Re}(-i\tilde{t}_{66})$  with  $\text{Re } t_{66}^2$  at the point where they have their maximum strength which happens to be close the  $M^*$  pole. In this way we avoid improper comparisons due to the small shifts in the apparent peak position of the different channels. Similarly, we can also compare  $\text{Im}(-i\tilde{t}_{66})$  with  $\text{Im}(t_{66})^2$  around 20 MeV above the apparent  $M^*$  position in each case, where these magnitudes have also maximum relative strength. Differences from both methods give us an idea about the intrinsic uncertainties in the determination of  $C$ . Hence we take

$$C \vec{\sigma} \cdot \vec{q}' \simeq g^2 \frac{\text{Re}(-i\tilde{t}_{66})}{\text{Re}(t_{66}^2)} \simeq g^2 \frac{\text{Im}(-i\tilde{t}_{66})}{\text{Im}(t_{66}^2)}. \quad (37)$$

Our technical procedure will be to evaluate  $\tilde{t}_{66}$  from the series of Fig. 5 and apply eq. (37), using the amplitude  $t_{66}$  provided by the model of section 2. It is not difficult to see that the  $\tilde{t}_{66}$  amplitude for an external  $\pi^0$  is evaluated by

$$\begin{aligned} -i\tilde{t}_{66} = & \sum_{l,m} t_{6l} G_l D_{lm\pi^0} \vec{\sigma} \cdot \vec{q}' G_m t_{m6} + \sum_l t_{6l} \tilde{G}_l A_l \vec{\sigma} \cdot \vec{q}' t_{l6} \\ & + t_{62} \tilde{G}^* A_{\Sigma^0 \Lambda \pi^0} \vec{\sigma} \cdot \vec{q}' t_{36} + t_{63} \tilde{G}^* A_{\Sigma^0 \Lambda \pi^0} \vec{\sigma} \cdot \vec{q}' t_{26}, \end{aligned} \quad (38)$$

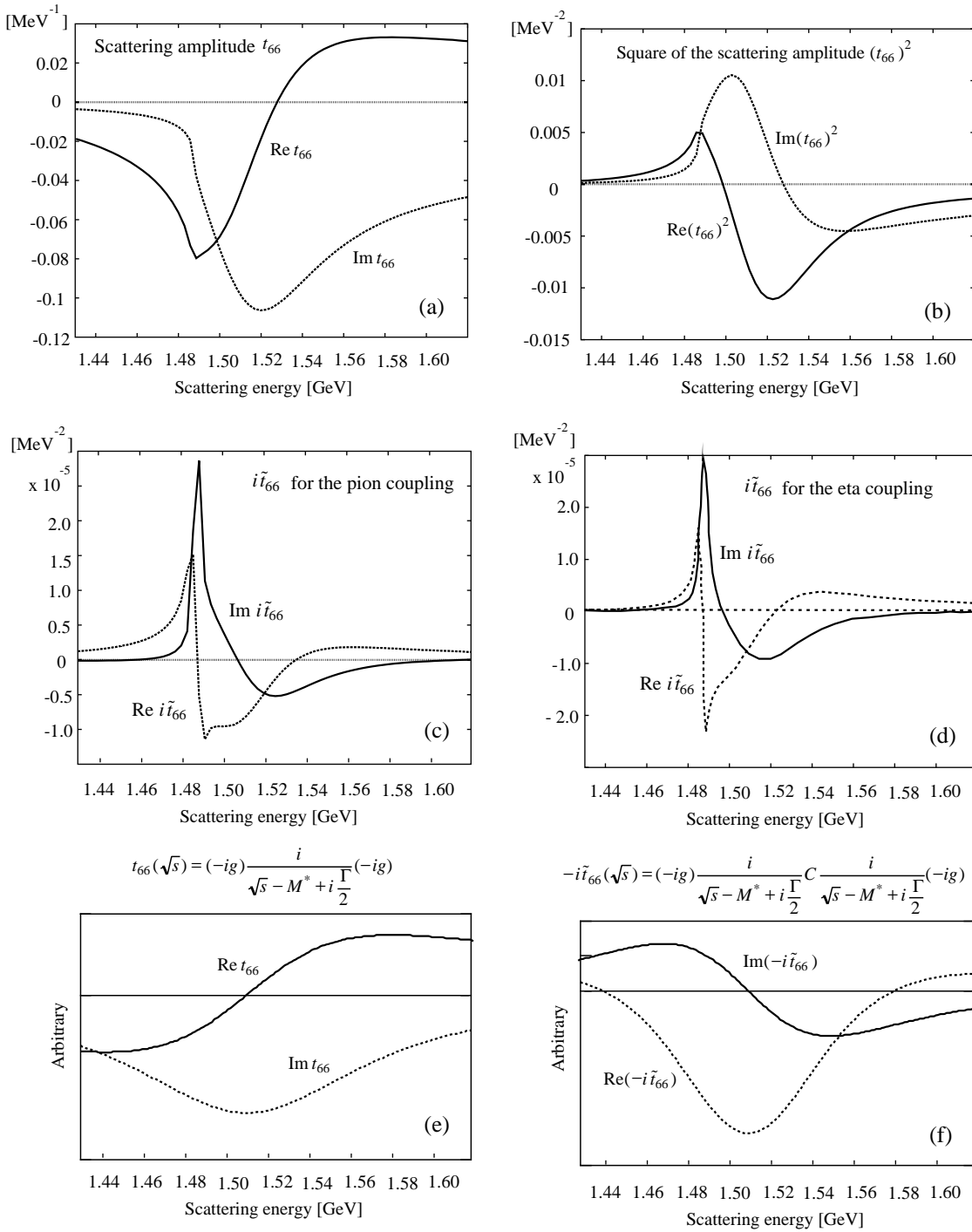


Figure 11: Real and imaginary parts of various scattering amplitudes as functions of scattering energy  $\sqrt{s}$ : (a)  $t_{66}$ , (b)  $(t_{66})^2$ , (c)  $i \tilde{t}_{66}$  for the pion coupling, (d)  $i \tilde{t}_{66}$  for the eta coupling, (e) the Breit-Wigner amplitude for  $t_{66}$ , and (f) the Breit-Wigner amplitude for  $-i \tilde{t}_{66}$ . In  $-i \tilde{t}_{66}$  of (c), (d) and (f), the factor  $\vec{\sigma} \cdot \vec{q}'$  is removed. The difference in signs of (c), (d) and (f) accounts for the isospin factor coming from the  $\pi^0 n^* n^*$  coupling, where  $n^*$  is the neutron  $N^*(1535)$ .

where

$$\tilde{G}_l = i \int \frac{d^4 q}{(2\pi)^4} \frac{M_l}{E_l(\vec{q})} \frac{M_l}{E_l(\vec{q})} \left( \frac{1}{\sqrt{s} - q^0 - E_l(\vec{q}) + i\epsilon} \right)^2 \frac{1}{q^2 - m_l^2 + i\epsilon}. \quad (39)$$

Here by taking  $q'^\mu \rightarrow 0$ , the square of the baryon propagator appears. The coefficients  $D_{lm\pi^0}$  in eq. (38) are given by eq. (30), and the coefficients  $A_l$  are abbreviations for  $A_{ll\pi^0}$ . The last two terms in eq. (38) correspond to Fig. 5(c) with intermediate  $\Sigma^0$ ,  $\Lambda$  or  $\Lambda$ ,  $\Sigma^0$  respectively. For the meson baryon propagator  $\tilde{G}^*$  we take here the same formula as eq. (39) with an average mass for the  $\Lambda$  and the  $\Sigma^0$ . Since there is no  $\Sigma^0\Lambda\eta$  coupling, these last two terms in eq. (38) do not appear for the case of the external  $\eta$ .

By taking one of the  $M/E$  factors unity, we can obtain  $\tilde{G}_l$  from  $G_l$  by differentiating with respect to  $\sqrt{s}$ . Hence

$$\tilde{G}_l = -\frac{\partial G_l}{\partial \sqrt{s}}. \quad (40)$$

It is clear that in this procedure there is some element of arbitrariness because in order to evaluate  $G_l$  we have fixed the cut off arbitrarily and adjusted the  $a_l$  coefficients to the data. Since  $a_l$  is a constant it will not contribute in the derivative of eq. (40). In order to estimate uncertainties from this procedure we recast the expressions for  $G_l$ , omitting the term  $a_l$  and putting an equivalent cut off  $q_{max}$  such that the same value of  $G_l$  at the energy of the resonance is obtained. We have tested it in the case of the  $K\Sigma$  channel. In this case the enlarged range of the integral provides some contribution to eq. (40) when differentiating with respect to  $\sqrt{s}$ . However, since the new region of integration, far off shell, has a weak dependence on  $\sqrt{s}$ , this leads to stable results. In this case the equivalent cut off is of order 6 GeV, but the changes in  $\partial G / \partial \sqrt{s}$  only influence the value of the  $C$  coefficient at the level of 1%. This procedure cannot be applied to other channels, since we cannot find an equivalent cut off larger than the on shell value of the momentum in the loop. The small correction found in the feasible case is the basis why we expect that the procedure adopted by means of eq. (40) is a fair one.

## 5 Results and discussions

### 5.1 Numerical results

As we explained in section 3, we consider the zero charge state for  $N^*(1535)$ . The evaluation of the  $C$  coefficient for  $\pi^0 N^* N^*$  gives us:

$$C_{\pi^0 N^* N^*} = -8.4 \cdot 10^{-3} \text{ MeV}^{-1} \quad (-9.3 \cdot 10^{-3} \text{ MeV}^{-1}), \quad (41)$$

where the first number is the ratio of the real parts in eq. (37), while that in the parenthesis the one of imaginary parts. We shall take the average of the two  $-8.9 \cdot 10^{-3} \text{ MeV}^{-1}$ .

The number  $C$  in eq. (41) should be compared with the equivalent coupling  $\pi^0 NN$ , which is given by  $-\frac{D+F}{2f}$  with  $D+F = 1.26 = g_A$ . Hence we find

$$\frac{C_{\pi^0 N^* N^*}}{C_{\pi^0 NN}} \sim 1.3, \quad (42)$$

which tells us that the  $N^* N^* \pi$  and  $NN\pi$  coupling have about the same strength and equal signs. Hence this would rule out the possibility of the mirror assignment. Using the ratio of the Goldberger-Treiman relations for  $N$  and  $N^*$

$$g_A^* = \frac{M}{M^*} \frac{C_{\pi^0 N^* N^*}}{C_{\pi^0 NN}} g_A, \quad (43)$$

one can relate the number of (42) to  $g_A^*$ :

$$g_A^* \sim 1. \quad (44)$$

In order to have some feeling for the strength of the different terms we summarize here the general trends of the numerics.

*i)* We get a contribution to  $\text{Re } C$  of the same sign from the first two terms in eq. (38). The strength of the term with the  $GDG$  combination is about twice as large as the one from  $\tilde{G}_l$ . In terms of diagrams, (a)(b) of Fig. 5 combined are more important than the diagram (c).

*ii)* We find that, in the  $GDG$  combinations, the contribution of the loops with  $K\Sigma$  or  $K\Lambda$  is about one order of magnitude smaller than the corresponding one with a  $\pi N$  loop.

*iii)* The only relevant contribution of diagram (b) of Fig. 5 involving the  $\tilde{X}, \tilde{Y}$  coefficients comes from the two  $\pi^- p$  loops, with the rest being negligible. This contribution is about three times larger than the corresponding one from diagram (a) involving the  $X, Y$  coefficients.

*iv)* The contribution from the different loops to the  $\tilde{G}_l$  terms has about the same strength for all channels involving two equal baryons in the diagram (c) of fig. 5. However the terms involving  $\Sigma^0, \Lambda$  intermediate states contribute at the level of 10%.

As for the  $\eta$  coupling we obtain

$$C_{\eta N^* N^*} = -14.0 \cdot 10^{-3} \text{ MeV}^{-1} \quad (-15.5 \cdot 10^{-3} \text{ MeV}^{-1}). \quad (45)$$

where the two numbers correspond to the ratio of real and imaginary parts in eq. (36). As in the case of the  $\pi^0$  we take also the average value  $-14.7 \cdot 10^{-3} \text{ MeV}^{-1}$ , which gives a ratio

$$\frac{C_{\eta N^* N^*}}{C_{\pi^0 NN}} = 2.2. \quad (46)$$

The strength of the  $\eta$  coupling here appears to be nearly twice the corresponding one of the pion, but as discussed above we should admit larger uncertainties here than in the case of the  $\pi^0$  coupling.

We can rewrite the coefficients  $C_{\pi^0 N^* N^*}$  and  $C_{\eta N^* N^*}$  in terms of the  $F'$ ,  $D'$  coefficients of SU(3), assuming the  $N^*(1535)$  to be equivalent of the N in an octet of excited baryons. By analogy to eq. (16) we would have

$$C_{\pi^0 N^* N^*} = -\frac{D' + F'}{2f} = -1.3\left(\frac{D + F}{2f}\right) \quad (47)$$

$$C_{\eta N^* N^*} = \frac{1}{\sqrt{3}}\frac{D' + F'}{2f} - \frac{2}{\sqrt{3}}\frac{D' - F'}{2f} = -2.2\left(\frac{D + F}{2f}\right) \quad (48)$$

These equations are compatible with

$$D' \simeq 2.4, \quad (49)$$

$$F' \simeq -0.79, \quad (50)$$

from which one could obtain the different  $B'BM$  couplings for the excited baryon states.

The value of  $D'$  is about three times the value of  $D$  for the coupling with the nucleon and the value of  $F'$  has a strength about twice bigger than  $F$  and has opposite sign. We should note that the uncertainty in the  $N^*N^*\eta$  coupling has repercussions mostly on  $F'$ . Indeed, if we decrease  $C_{N^*N^*\eta}$  by 30%  $D'$  decreases only by 15% but  $F'$  is reduced to about half its value in eq. (50).

## 5.2 Comparison with other models

It would be interesting to compare the present result with other model calculations. There are several examples which appear to support the present result.

First we discuss the implications of the non-relativistic (NR) quark model, where the negative parity baryons emerge as orbitally excited states of  $l = 1$  ( $p$  state). There are two independent states for  $1/2^-$ :

$$\begin{aligned} |1\rangle &= [l = 1, S = 1/2]^{1/2^-}, \\ |2\rangle &= [l = 1, S = 3/2]^{1/2^-}, \end{aligned} \quad (51)$$

where the  $p$  state is coupled either by the total spin  $S = 1/2$  state or  $S = 3/2$ . In the presence of a tensor force, these two states are mixed and their linear combinations are interpreted as physical resonances:

$$|N^*(1535)\rangle = a|1\rangle - b|2\rangle, \quad (52)$$

$$|N^*(1650)\rangle = b|1\rangle + a|2\rangle. \quad (53)$$

Here the coefficients  $a$  and  $b$  are real and satisfy  $a^2 + b^2 = 1$  ( $b > 0$ ).

The axial vector coupling constant is then defined by

$$g_A^* = \langle p^*(1535), s_z = 1/2 | \sum_{i=1,2,3} \sigma_3^{(i)} \tau_3^{(i)} | p^*(1535), s_z = 1/2 \rangle, \quad (54)$$

where  $\sigma^{(i)}$  and  $\tau^{(i)}$  are quark spin and isospin matrices for the  $i$ -th quark and the sum runs over the three quarks. The matrix element of eq. (54) is easily computed and the result is

$$g_A^* = \frac{1}{9} (-a^2 + 16a\sqrt{1-a^2} + 5(1-a^2)). \quad (55)$$

In Fig. 12 we show  $g_A^*$  as a function of the mixing coefficient  $a$ . We see that depending on the value of  $a$ , the coupling constant  $g_A^*$  can be either positive or negative. In the successful model by Isgur and Karl [24], the mixing coefficient takes the value  $a \sim 0.85$ , yielding the axial vector coupling constant  $g_A^* \sim 0.87$ , which compares well with the present result  $g_A^* \sim 1$  in eq. (44).

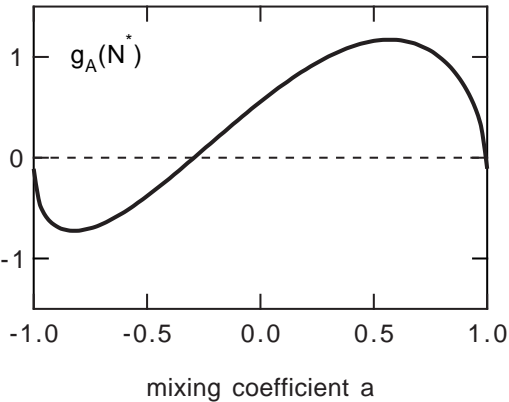


Figure 12:  $g_A^*$  as a function of the mixing coefficient  $a$ .

Another interesting case is presented by the large- $N_c$  consideration. A somewhat nontrivial assumption here is the hedgehog correlation, where spin and isospin degrees are strongly correlated such that the intrinsic state acquire the grand spin  $\vec{K} = \vec{J} + \vec{I} = 0$ . Here  $J$  is the total spin,  $\vec{J} = \vec{L} + \vec{S}$ , and  $\vec{I}$  the isospin. In the large- $N_c$  limit, quark-quark interactions become small as the Hartree approximation becomes exact. Hence the hedgehog configuration is assumed for each quark separately. For  $s$  and  $p$  quarks, such hedgehog states are

$$|h\rangle = [s, \tau]^K = [1/2, 1/2]^0, \quad (56)$$

$$|h^*\rangle = [[l, s]^j, \tau]^K = [[1, 1/2]^{1/2}, 1/2]^0. \quad (57)$$

Hence the negative parity hedgehog for  $N^*(1535)$  in the large- $N_c$  limit takes the form

$$|H\rangle = \frac{1}{N_c} (|h^* h \cdots h\rangle + \cdots |h \cdots h, h^*\rangle). \quad (58)$$

Physical baryon states are projected out from the hedgehog state by applying the projection operator:

$$|B\rangle \sim \int d[\omega] D_B^*(\omega) R^\tau(\omega) |H\rangle, \quad (59)$$

where  $R^\tau(\omega)$  is the rotation operator in isospin space and  $D_B^*(\omega)$  the  $D$ -function for a physical baryon state  $B$ .

For  $N_c = 3$  the integral in eq. (59) yields

$$|B = 1/2^-\rangle = \frac{1}{\sqrt{2}}(|1\rangle - |2\rangle), \quad (60)$$

where the states  $|1\rangle$  and  $|2\rangle$  are those given in eqs. (51). Thus the mixing coefficient  $a$  in this case is precisely  $1/\sqrt{2}$  and the corresponding  $g_A^* = 1.11$ . We note that this mixing rate is consistent with the result obtained in a phenomenological analysis based on the large- $N_c$  [25]. Therefore, the non-relativistic quark model, both in the Isgur-Karl and the large- $N_c$  approaches, yields the axial vector coupling constants for  $N^*$  which are consistent with the prediction of the chiral unitary model.

The last example is provided by the Skyrme model, where the  $N^*(1535)$  resonance can be constructed dominantly as an  $s$ -wave eta-nucleon bound state [26, 27]. When the original Skyrme model is extended minimally to the SU(3) case, the eta which is introduced as a fluctuation field feels an attractive potential around the Skyrme soliton. In the large  $N_c$  limit, the soliton solution appears in the leading order and the fluctuation field next to leading order does not affect the shape of the soliton solution. Therefore, the pion coupling which is determined from the tail behavior of the soliton solution takes the same form both for the nucleon and for  $N^*(1535)$ .

In the chiral limit  $m_\pi = 0$ , the strength of the asymptotic soliton profile  $F(r) \rightarrow b/r^2$  is related to the pion coupling and to the axial coupling through

$$\begin{aligned} g_{\pi N^* N^*} &= \frac{8\pi M^*}{3} f_\pi b, \\ g_A^* &= \frac{8\pi}{3} f_\pi^2 b, \end{aligned} \quad (61)$$

which are the same equations as those for the nucleon if the asterisk  $*$  is removed [28]. Therefore, using the parameters of Adkins-Nappi-Witten [29], we find

$$g_{\pi N^* N^*} = M^*/M_N g_{\pi NN} \sim 13.5 \quad (62)$$

and

$$g_A^* = 0.65 \quad (= g_A). \quad (63)$$

Once again, we find that both  $g_{\pi N^* N^*}$  and  $g_A^*$  take values consistent with that of the chiral unitary approach.

## 6 Conclusions

We have evaluated the  $N^*N^*\pi^0$  and  $N^*N^*\eta$  couplings using a chiral unitary approach where the  $N^*(1535)$  is generated dynamically. We could generate these couplings in terms of known couplings of the  $\pi$ ,  $\eta$  to baryons and other mesons as given by the chiral Lagrangians. The values obtained are of the same order of magnitude as the  $\pi NN$  coupling. In the case of the  $\pi N^*N^*$  coupling we get the same sign as the  $\pi NN$  one. This is the sign expected for the naive assignment in the chiral doublet combining mesons and baryons. The uncertainties in the approach followed here can not reverse this sign, hence the present calculations appear to rule out the mirror case.

We have compared the present result with other models for  $N^*$ , e.g., the non-relativistic quark model of Isgur-Karl, the large- $N_c$  approach and the Skyrme model. We have found that all of them predict similar values for  $g_{\pi N^*N^*}$  and  $g_A$  with the same sign. Hence,  $N^*(1535)$  which appears as the first resonance state in the pion (and eta) scatterings is likely to carry a naive chiral assignment together with the ground state nucleon.

It would be further interesting if we can confirm our theoretical implication in experiments. Since we can not have a stable target for  $N^*(1535)$ , the measurement of coupling constants will necessarily require somewhat complicated processes. One such candidate is to measure a two meson production of the pion and eta simultaneously. The eta meson can be used as a probe for the production of  $N^*(1535)$ . Then, another pion can be produced either at the  $N^*(1535)$  or at the nucleon with the coupling constant  $g_{\pi N^*N^*}$  and  $g_{\pi NN}$ , respectively, as illustrated in Fig. 13. Depending on the sign of the two couplings, the two terms can be added either constructively or destructively. One may use such coherent processes to see the relative sign of the two coupling constants [13].

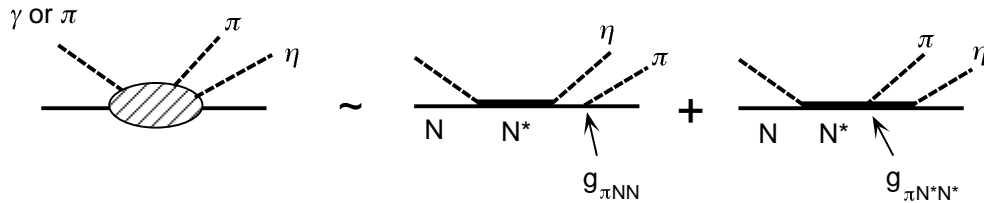


Figure 13: A resonance dominant process for the two meson production of  $\pi$  and  $\eta$ .

We have also calculated the corresponding SU(3) coefficients  $D'$  and  $F'$ , which would allow one to calculate the  $B'BM$  couplings with the octet of excited baryon states to which the  $N^*(1535)$  belongs and the mesons of the  $0^-$  stable octet. The value obtained for  $D'$  is about three times the value of  $D$  while the value of  $F'$  is about twice the one of  $F$  and of opposite sign. We should, however, note that  $F'$  has larger uncertainty than  $D'$ .

The exercise done here has also served to show how one can technically implement the coupling of an external pion or eta to a resonance structure. These techniques can easily be generalized to obtain the coupling of other external sources as photons, vector mesons, etc, which would enable one to evaluate magnetic moments of resonances and other electromagnetic or weak properties.

## Acknowledgments

We are grateful to the COE Professorship program of Monbusho, which enabled E. O. to stay at RCNP to perform the present work. Useful discussions and ideas from J. A. Oller are much appreciated. A.P. would like to acknowledge Prof. R.A. Arndt and N. Kaiser for providing her with some experimental data and other helpful information. A.H. and M.O thank D. Jido for discussions on  $\pi$  and  $\eta$  productions. J.C. Nacher would like to acknowledge the hospitality of the RCNP of the Osaka University where this work was done and support from the Ministerio de Educación y Cultura. This work is partly supported by DGICYT contract number PB96-0753 and PB95-1249, and also by DOE Grant DE-FG06-91ER40561.

## References

- [1] S. Coleman, *Aspects of Symmetry*, Cambridge University Press, Cambridge (1985).
- [2] J. Gasser and H. Leutwyler, Nucl. Phys. B250 (1985) 465
- [3] U. G. Meissner, Rep. Prog. Phys. 56 (1993) 903
- [4] A. Pich, Rep. Prog. Phys. 58 (1995) 563
- [5] G. Ecker, Prog. Part. Nucl. Phys. 35 (1995) 1
- [6] V. Bernard, N. Kaiser and U. G. Meissner, Int. J. Mod. Phys. E4(1995)193
- [7] J. A. Oller, E. Oset and J. R. Peláez, Phys. Rev. Lett. 80(1998)3452; Phys. Rev. D 59(1999)71001
- [8] F. Guerrero and J. A. Oller, Nucl. Phys. B 537(1999)459
- [9] J. A. Oller and E. Oset, Nucl. Phys. A620(1997)438; erratum Nucl. Phys. A in print.
- [10] J. A. Oller and E. Oset, submitted to Phys. Rev. D, hep-ph/9809337
- [11] G. Ecker, J. Gasser, A. Pich and E. de Rafael, Nucl. Phys. B321 (1989) 311

- [12] D. Jido, M. Oka and A. Hosaka, Physical Review Letters, 80 (1998) 448.
- [13] D. Jido, Y. Nemoto, M. Oka and A. Hosaka, Preprint, 80 (1998) 448.
- [14] H. Kim, D. Jido and M. Oka, Physical Review Letters, 80 (1998) 448.
- [15] N. Kaiser, P. B. Siegel and W. Weise, Phys. Lett. B 362(1995)23
- [16] N. Kaiser, P. B. Siegel and W. Weise, Nucl. Phys. A594 (1995) 325
- [17] N. Kaiser, T. Waas and W. Weise, Nucl. Phys. A612 (1997) 297
- [18] E. Oset and A. Ramos, Nucl. Phys. A635(1998)99
- [19] A. Parreño, A. Ramos and E. Oset in preparation
- [20] M. Roos, Phys. Lett. B246 (1990) 179.
- [21] R. A. Arndt, A. M. Green, R. L. Workman and S. Wycech, Phys. Rev. C58(1998)3636
- [22] U. G. Meissner, E. Oset and A. Pich, Phys. Lett. B353(1995)161
- [23] S. Weinberg, Phys. Rev. Lett. 18(1967)188
- [24] N. Isgur and G. Karl, Phys. Lett. 72B (1977) 109; *ibid.* 74B (1978) 353; Phys. Rev. D18 (1978) 4187; *ibid.* D20 (1979) 1191.
- [25] C.D. Carone, H. Georgi, L. Kaplan and D. Morin, Phys.Rev. D50 (1994) 5793.
- [26] G. Pari, Phys. Lett. B261 (1991) 347.
- [27] A. Hosaka, Phys. Lett. B293 (1992) 23; *ibid.* B306 (1993) 207.
- [28] A. Hosaka and H. Toki, Phys. Reports, 277 (1996) 65.
- [29] G.S. Adkins, C.R. Nappi and E. Witten, Nucl. Phys. B228 (1984) 552.